



ELSEVIER

Contents lists available at ScienceDirect

Chemical Geology

journal homepage: [www.elsevier.com/locate/chemgeo](http://www.elsevier.com/locate/chemgeo)

## Ecosystem controlled soil-rock $p\text{CO}_2$ and carbonate weathering – Constraints by temperature and soil water content

G. Romero-Mujalli<sup>a,\*</sup>, J. Hartmann<sup>a</sup>, J. Börker<sup>a</sup>, J. Gaillardet<sup>b</sup>, D. Calmels<sup>c</sup>

<sup>a</sup> Institute for Geology, Department of Earth Science, Center for Earth System Research and Sustainability (CEN), Universität Hamburg, Bundesstraße 55, 20146 Hamburg, Germany

<sup>b</sup> Institut de Physique du Globe de Paris, Sorbonne Paris Cité, CNRS and Institut Universitaire de France, Paris, France

<sup>c</sup> Université Paris-Sud, Laboratoire GEOPS, UMR 8148 – CNRS, Orsay F-91405, France

### ARTICLE INFO

#### Keywords:

Hydrogeochemistry  
Soil carbon dioxide  
Carbonate weathering  
Inverse calculation

### ABSTRACT

Carbonate dissolution in soil-groundwater systems depends dominantly on pH, temperature and the saturation state of the solution with respect to abundant minerals. The pH of the solution is, in general, controlled by partial pressure of  $\text{CO}_2$  ( $p\text{CO}_2$ ) produced by ecosystem respiration, which is controlled by temperature and water availability. In order to better understand the control of land temperature on carbonate weathering, a database of published spring water hydrogeochemistry was built and analysed. Assuming that spring water is in equilibrium with the soil-water-rock-atmosphere, the soil  $p\text{CO}_2$  can be back-calculated. Based on a database of spring water chemistry, the average soil-rock  $\text{CO}_2$  was calculated by an inverse model framework and a strong relationship with temperature was observed. The identified relationship suggests a temperature control on carbonate weathering as a result of variations in soil-rock  $p\text{CO}_2$ , which is itself controlled by ecosystem respiration processes. The findings are relevant for global scale analysis of carbonate weathering and carbon fluxes to the ocean, because concentration of weathering products from the soil-rock-system into the river system in humid, high temperature regions, are suggested to be larger than in low temperature regions. Furthermore, results suggest that, in specific spring samples, the hydrochemical evolution of rain water percolating through the soil-rock complex can best be described by an open system with  $p\text{CO}_2$  controlled by the ecosystem. Abundance of evaporites and pyrite sources influence significantly the chemistry of spring water and corrections must be taken into account in order to implement the inverse model framework presented in this study. Annual surface temperature and soil water content were identified as suitable variables to develop the parameterization of soil-rock  $p\text{CO}_2$ , mechanistically consistent with soil respiration rate findings.

### 1. Introduction

The production of carbon dioxide ( $\text{CO}_2$ ) in soils depends mostly on microbial activity and root respiration which in turn are dependent on temperature and soil water content, parameters representing climate variability (Amundson and Davidson, 1990; Kuzyakov, 2006; Lellei-Kovács et al., 2016; Mielnick and Dugas, 2000). Soil respiration is a major component in the carbon cycle and is considered to be one of the largest biological  $\text{CO}_2$  fluxes from land to the atmosphere (Raich and Potter, 1995). Nevertheless, soil  $\text{CO}_2$  when dissolved in water, represents the major hydronium ion supply in the weathering system, and it is consumed through weathering reactions (Berner et al., 1983; Calmels et al., 2014; Walker et al., 1981).

Quantifying the weathering fluxes from land to the coastal zone is of interest to understand the atmospheric/soil  $\text{CO}_2$  consumption potential

through chemical weathering. Several authors have tried to constrain these fluxes studying the chemistry of large rivers (Gaillardet et al., 1999), using phenomenological models to determine global weathering fluxes for different types of lithological classes (Bluth and Kump, 1994; Goll et al., 2014; Hartmann, 2009; Hartmann et al., 2009; Hartmann et al., 2014; Suchet and Probst, 1993), or applying mechanistic models based on kinetic equations and hydrology to quantify the weathering fluxes from soil-rock system to the rivers (Beaulieu et al., 2012; Goddérís et al., 2013; Goddérís et al., 2006; Roelandt et al., 2010). Nevertheless, the mechanistic models require as an important input the soil partial pressure of  $\text{CO}_2$  ( $p\text{CO}_2$ ), which controls the saturation state with respect to minerals and therefore the amount of minerals that can be dissolved.

The weathering of carbonate rocks is a dynamic process and variations on timescales of hours are documented, as well as fast

\* Corresponding author.

E-mail address: [gibran.romero.mujalli@uni-hamburg.de](mailto:gibran.romero.mujalli@uni-hamburg.de) (G. Romero-Mujalli).

<https://doi.org/10.1016/j.chemgeo.2018.01.030>

Received 5 January 2017; Received in revised form 27 October 2017; Accepted 26 January 2018

0009-2541/© 2018 The Authors. Published by Elsevier B.V. This is an open access article under the CC BY-NC-ND license (<http://creativecommons.org/licenses/by-nc-nd/4.0/>).

precipitation, mainly dependent on the concentration of  $\text{CO}_2$  in the aqueous system (Calmels et al., 2014; Pu et al., 2013; Roland et al., 2013; Serrano-Ortiz et al., 2010). The fast calcite dissolution implies that equilibrium is easily reached with respect to a given  $p\text{CO}_2$  (Dreybrodt et al., 1996; Reddy et al., 1981) without expecting fast calcite precipitation due  $\text{CO}_2$  degassing in the spring water (Szramek and Walter, 2004). As a consequence, the alkalinity in spring water presents the spatio-temporal variation of  $\text{CO}_2$  of its catchment source system (Calmels et al., 2014; Yoshimura et al., 2001). In that way, the concentration of chemical species resulting from carbonate weathering might be a good parameter to forecast the soil  $p\text{CO}_2$  in a soil-carbonate rock-system.

There are, at least theoretically, two extreme models to describe carbonate dissolution. The “open system” corresponds to an infinite  $\text{CO}_2$  reservoir that equilibrates with the dissolving solution (or sustained supply of  $\text{CO}_2$ ). The “closed system” corresponds to the case where a given initial amount of  $\text{CO}_2$  equilibrates with the solution and no further supply is provided. In both cases,  $\text{CO}_2$  is consumed through the weathering reaction according to the chemical equations of the carbonate system until saturation with respect to calcite is reached. Although both cases should exist in reality, the soil-carbonate rock weathering system more likely operates as an open system because (i) an ongoing flux of  $\text{CO}_2$ , due to the ecosystem respiration and microbial activity, might be expected and (ii) the dissolution of calcium carbonate rocks is a relatively fast process.

The aim of this study is to back-calculate the soil-rock  $p\text{CO}_2$  based on equilibrium equations and considering open and closed conditions for carbonate dominated lithologies, using spring water chemistry. In addition, a framework to retrieve a generalized soil-rock  $p\text{CO}_2$  function for carbonate rock dominated areas based on land properties sensitive to climate variability is presented.

## 2. Methodology

### 2.1. Spring water chemistry and data filtering

A spring database for carbonate lithologies was constructed based on publications where carbonates rocks are considered an important lithological class in the catchment and information of the chemistry of the water was available (Fig. 1). The database is composed of 671 data points from 26 different publications and sampling locations are located approximately between latitudes  $20^\circ$  and  $60^\circ$  N. For each sample point an estimate of the coordinates was determined.  $\delta^{13}\text{C}$  data, when reported, was included in the database (Supplement information) because it can be used to determine the source of  $\text{CO}_2$ , degassing processes and

to identify the influence of redox processes.

Some studies reported water chemistry data from hot or cold springs where  $\text{CO}_2$  from deep sources and hydrothermal processes is likely (Chiodini et al., 1999; Herman and Lorah, 1987; Kohfahl et al., 2008; Yoshimura et al., 2004; Yoshimura et al., 2001). In this case, the  $p\text{CO}_2$  in the soil-rock system is not representative of the soil  $\text{CO}_2$  produced by the ecosystems. Therefore, filtering of data is needed in order to select samples with ideal conditions characteristic of the interactions between the Ca-carbonate rock, water and the ecosystem. In addition, sulfide oxidation and gypsum dissolution may change the alkalinity of the solution interacting with carbonate. If silicates are present in the catchment, they may add excess alkalinity. In order to minimize the influence of evaporites, sulfide oxidation processes or hydrothermal processes the following filtering criteria were applied:

- (i)  $([\text{Ca}^{2+}] + [\text{Mg}^{2+}])/\text{alkalinity}$  molar ratio  $< 0.9$ , in order to discard the extreme values shown in Fig. 2a, where these cations may be related to a source other than carbonate minerals by soil  $\text{CO}_2$ .
- (ii)  $[\text{Ca}^{2+}]/[\text{SO}_4^{2-}]$  molar ratio should be  $> 10$  (Fig. 2b), to discard samples affected by sulfide oxidation and sulfate mineral dissolution.
- (iii)  $[\text{Ca}^{2+}]/[\text{Na}^+]$  molar ratios should be  $> 12$ , in order to minimize the effect silicate weathering (Fig. 2c), based on Gaillardet et al. (1999) relations and data analysis reported therein.
- (iv)  $[\text{Ca}^{2+}]/[\text{Mg}^{2+}]$  molar ratio should be larger than 1, to minimize contribution of other carbonate minerals than calcite and silicate minerals (Fig. 2d), and to be able to apply equilibrium equations for calcite dissolution system.
- (v) The charge balance error (CBE) should be  $< 10\%$ , to exclude points with high uncertainty associated to the reported water chemistry data. CBE was calculated by the following equation:

$$\text{CBE} = \frac{\sum_{p=1}^n C_{e_p} - \sum_{j=1}^m C_{e_j}}{\sum_{p=1}^n C_{e_p} + \sum_{j=1}^m C_{e_j}} * 100 \quad (1)$$

where  $C_{e_p}$  and  $C_{e_j}$  represent the concentration in equivalent of cation  $p$  and anion  $j$ , respectively. A more rigorous condition for CBE was not necessary to apply because the deviation due seasonality is larger.

Correction for rain water was not possible due to lack of information on the chemistry of rainwater at each sample site but given the low pH of rainwater, the input of alkalinity by rain water is negligible. Seasonality was not considered due to limitation on the dataset and because the applied data for land temperature and soil water content implemented was based on year average. The chemistry of the selected spring samples (164 in total) is dominated by  $[\text{Ca}^{2+}]$  and alkalinity, an important condition to apply simple equilibrium calculations of the

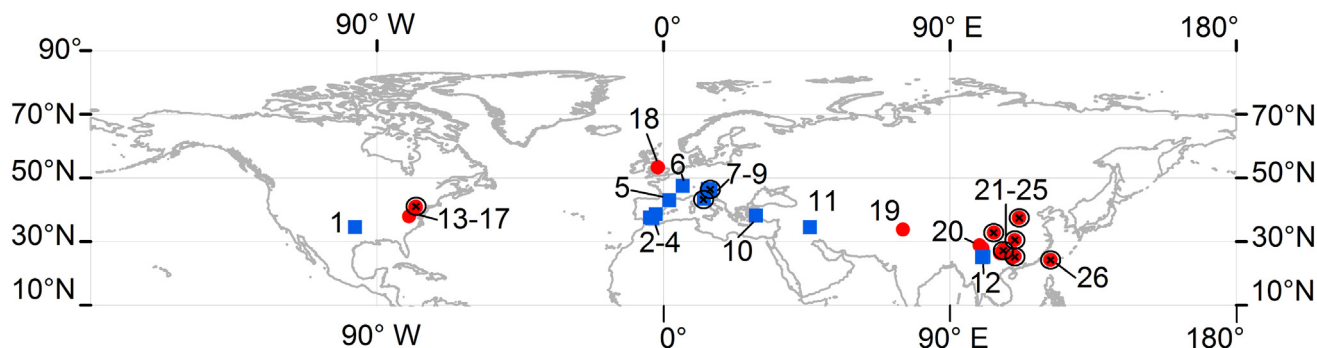
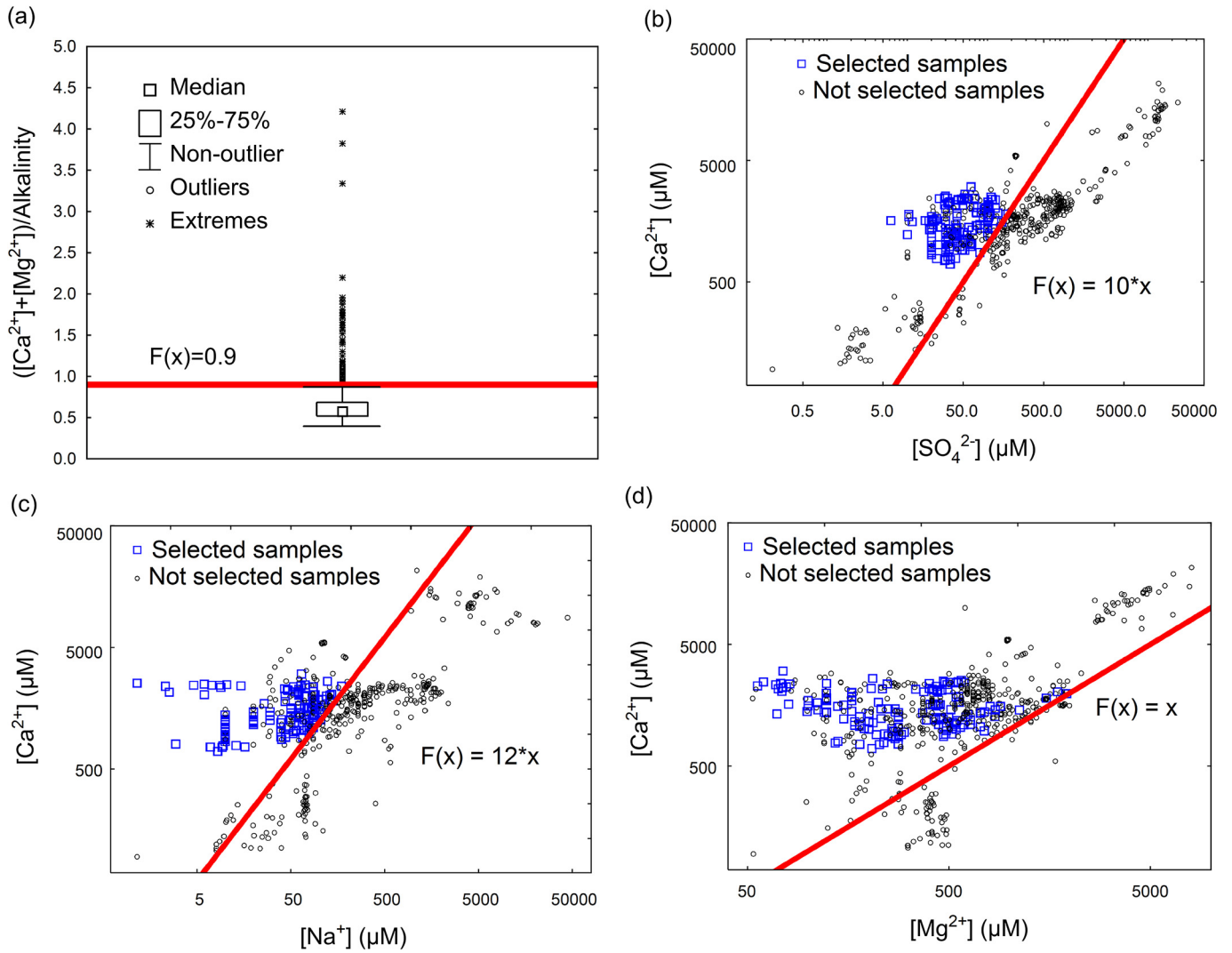


Fig. 1. Global distribution of the spring samples considered in the present study. Blue squares represent publications which fulfil the conditions proposed in the methodology, red circles correspond to publications with no measurements satisfying the conditions, and the black X marks stand for publications where  $\delta^{13}\text{C}$  measurements in water were reported. 1 = Abongwa and Atekwana (2015). 2 = Lopez-Chicano et al. (2001). 3 = Kohfahl et al. (2008). 4 = Moral et al. (2008). 5 = Dandurand et al. (1982). 6 = Calmels et al. (2014). 7 = Chiodini et al. (1999). 8 = Kanduč et al. (2012). 9 = Szramek et al. (2011). 10 = Özkul et al. (2010). 11 = Karimi et al. (2005). 12 = Huang et al. (2015). 13 = Herman and Lorah (1987). 14 = Jacobson and Langmuir (1970). 15 = Langmuir (1971). 16 = Deines et al. (1974). 17 = Jacobson and Langmuir (1974). 18 = Smith and Wood (2002). 19 = Jeelani et al. (2011). 20 = Pu et al. (2013). 21 = Zhao et al. (2015). 22 = Zaihua et al. (1997). 23 = Yoshimura et al. (2004). 24 = Long et al. (2015). 25 = Qibo et al. (2016). 26 = Yoshimura et al. (2001). (For interpretation of the references to colour in this figure legend, the reader is referred to the web version of this article.)

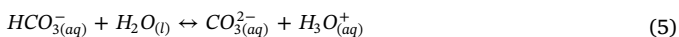
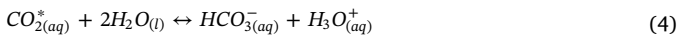


**Fig. 2.** Molar ratios and relations between chemical species: Graph (a) represents the box-plot of  $([Ca^{2+}] + [Mg^{2+}])$ /alkalinity molar ratio; and graphs (b), (c) and (d) are logarithm scale-scatterplots for  $[Ca^{2+}]$  against  $[SO_4^{2-}]$ ,  $[Na^+]$  and  $[Mg^{2+}]$ , respectively.  $F(x)$  stands for the selection criteria for each corresponding molar ratio and blue squares represent the samples which fulfil the conditions proposed in the methodology. (For interpretation of the references to colour in this figure legend, the reader is referred to the web version of this article.)

system  $CaCO_3$ - $H_2O$ - $CO_2$ .

## 2.2. Model description

A numerical code was constructed to calculate the  $pCO_2$  at equilibrium with spring samples considering the open system calcite- $CO_2$ -water, composed of the following chemical reactions:



where  $CO_{2(aq)}^*$  is the sum of species  $CO_{2(aq)}$  and  $H_2CO_{3(aq)}$ . The standard equilibrium constants ( $K$ ) at 25 °C of each chemical equation are reported in Table 1. The temperature dependency of the equilibrium constants and the Henry's constant was calculated using the van't Hoff equation (Eq. (7)), given by:

**Table 1**

Solubility product constants at 25 °C ( $K$ ) and standard enthalpy ( $\Delta H^\circ$ ) for the reactions considered in this work.

Reaction number	Constant ( $K$ )	$\Delta H^\circ$ (kJ mol <sup>-1</sup> )
Eq. (2)	$10^{-14}$	55.9066
Eq. (3)	$10^{-1.468a}$	-19.983
Eq. (4)	$10^{-6.352}$	9.109
Eq. (5)	$10^{-10.329}$	14.90
Eq. (6)	$10^{-8.48}$	-9.61

Thermodynamic data was taken from phreeqc.dat (Parkhurst and Appelo, 1999).

<sup>a</sup> Henry's constant for dissolution of gas  $CO_2$  in water.

$$\ln\left(\frac{K_k}{K_l}\right) = -\frac{\Delta H^\circ}{R} \left(\frac{1}{T_k} - \frac{1}{T_l}\right) \quad (7)$$

where  $T$  represents the absolute temperature in Kelvin,  $\Delta H^\circ$  the standard enthalpy of reaction and  $R$  the gas constant. Subscripts  $k$  and  $l$  indicate the different temperatures for each equilibrium constants.

The activity coefficient of each chemical species  $i$  ( $\gamma_i$ ) was calculated using Davies Equation (Eq. (8)):

$$\log \gamma_i = -Az_i^2 \left( \frac{\sqrt{I}}{1 + \sqrt{I}} - 0.3I \right) \quad (8)$$

where  $A$  is a temperature related constant,  $z_i$  is the charge of the chemical species and  $I$  is the ionic strength of the solution calculated using major compounds reported for each sample.

This model calculates the  $p\text{CO}_2$  required to produce the alkalinity values reported in each sample at the determined temperature assuming equilibrium with calcite. Alkalinity is considered to be  $[\text{HCO}_3^-] + 2[\text{CO}_3^{2-}] + [\text{OH}^-] - [\text{H}^+]$ , because no other chemical species with significant contribution to alkalinity were reported in the applied dataset. The construction of this model is based on three assumptions: (i) alkalinity values in spring waters dominated by weathering of carbonate lithologies depend, mainly, on the soil-rock  $p\text{CO}_2$ ; (ii) the system is at equilibrium with calcite (saturation index = 0); and (iii) ionic balance between chemical species  $[\text{H}^+]$ ,  $[\text{Ca}^{2+}]$ ,  $[\text{OH}^-]$ ,  $[\text{HCO}_3^-]$  and  $[\text{CO}_3^{2-}]$  was considered for all samples.

Furthermore, a closed-system calculation was carried out to determine the  $p\text{CO}_2$  required to produce the alkalinity values reported in the spring samples. In this case, the initial dissolved  $\text{CO}_2$  concentration, here as  $[\text{CO}_{2(\text{aq})}]_{\text{initial}}$ , was calculated as the sum of the  $\text{CO}_2$  at equilibrium in the closed system calcite-water- $\text{CO}_2$ ,  $[\text{CO}_{2(\text{aq})}]$ , plus the amount of  $\text{CO}_2$  which reacted with the calcite, which is equivalent to the calcium concentration,  $[\text{Ca}_{(\text{aq})}^{2+}]$ .

$$[\text{CO}_{2(\text{aq})}]_{\text{initial}} = [\text{Ca}_{(\text{aq})}^{2+}] + [\text{CO}_{2(\text{aq})}] \quad (9)$$

The  $p\text{CO}_2$  at equilibrium with the water (water  $p\text{CO}_2$ ) was calculated using PHREEQC software and “phreeqc.dat” database (Parkhurst and Appelo, 1999) and compared with the  $p\text{CO}_2$  estimated applying the inverse method presented in this study.

### 2.3. Global datasets

The calculated  $p\text{CO}_2$  was estimated by identifying suitable functional relationships using land surface temperature and soil volumetric water content, parameters often used for modelling the soil respiration (Cartwright and Hui, 2014; Epron et al., 1999; Gaumont-Guay et al., 2006; Mielnick and Dugas, 2000). Soil volumetric water content values were taken from the European Space Agency Climate Change Initiative data portal (ESA, <http://www.esa-soilmoisture-cci.org/>). This data, with a spatial resolution of 0.25°, represents the daily surficial water content of soils (depth < 5 cm) in volumetric units ( $\text{m}^3 \text{m}^{-3}$ ) calculated from the degree of saturation and soil porosity, and was developed by remote sensing methods which correlate the dataset with in-situ measurement stations (Dorigo et al., 2015; Liu et al., 2012; Wagner et al., 2012). Mean annual land surface temperature values with a spatial resolution of 1  $\text{km}^2$  were extracted from Hijmans et al. (2005). The calculated  $p\text{CO}_2$  was estimated using the annual mean soil volumetric water content ( $\theta$ ) and the global surface temperature by non-linear methods applying the Levenberg-Marquardt algorithm (functional relationships are discussed below).

## 3. Results

The compiled dataset is composed of 671 sample points representing different regions of the world where carbonate rocks dominate the catchment. Surface temperature and soil volumetric water content for the 164 selected spring samples range from 0.4 °C to 22.0 °C and from 0.17  $\text{m}^3 \text{m}^{-3}$  to 0.37  $\text{m}^3 \text{m}^{-3}$ , respectively. Subsequently, 164 sample points were selected based on the filtering method described in Section 2.1, centered on ideal carbonate dissolution signatures. The selected samples have calcite saturation indices (SI) between -0.4 to 1, with a mean value of 0.2. These samples present a moderate positive linear correlation between alkalinity and surface temperature ( $r^2 = 0.45$ , Fig. 3). This relationship is lost if the data selection is not applied, highlighting the difficulty of predicting and understanding

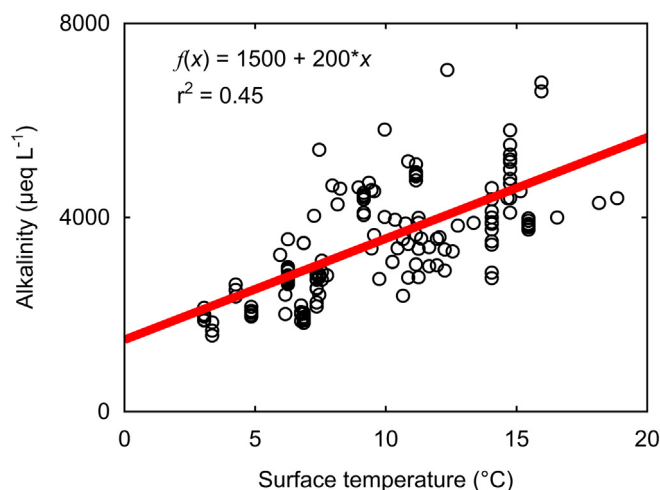


Fig. 3. Alkalinity against mean annual surface temperature for selected data points based on the conditions explained in Section 2.1.  $f(x)$  is the linear function of the correlation represented by the red line. (For interpretation of the references to colour in this figure legend, the reader is referred to the web version of this article.)

complex systems, where water chemistry is influenced by anthropogenic input and evaporite, sulfide or silicate mineral dissolution.

### 3.1. Stable carbon isotopes

Understanding the behaviour of stable carbon isotopes in spring water samples is useful to obtain information regarding the source of  $\text{CO}_2$  and possible processes occurring in the spring water system. From 671 total spring samples only 118 samples reported  $\delta^{13}\text{C}$  values, ranging from -20.6‰ to -0.3‰. Consequently, this variable was not used as imperative criteria for filtering the data. Nevertheless, the relationship between  $\delta^{13}\text{C}$  and alkalinity and pH allowed to distinguish at least two different groups (Fig. 4): a first group with relatively low values of  $\delta^{13}\text{C}$  (less than -4‰) and low alkalinity (< 8000  $\mu\text{eq L}^{-1}$ ) and a second group with elevated values of  $\delta^{13}\text{C}$  (higher than -5‰) and alkalinity values larger than 8000  $\mu\text{eq L}^{-1}$ .

Spring samples with high  $\delta^{13}\text{C}$  and alkalinity may be the result of the dissolution of calcite under the influence of  $\text{CO}_2$  from deep sources, or reaction of calcite with strong acids (Li et al., 2008; Yoshimura et al., 2004; Yoshimura et al., 2001), as implied by a generally lower pH values in Fig. 4b. Therefore, the  $\delta^{13}\text{C}$  was used as a minor condition to exclude samples possibly influenced by deep  $\text{CO}_2$  or hydrothermal processes. The resulting selected spring water samples present a good relationship between  $\delta^{13}\text{C}$  and alkalinity (Fig. 4a), where high values of  $\delta^{13}\text{C}$  are related to the lowest values of alkalinity reported in these spring samples. This may imply that the isotopic composition of soil  $\text{CO}_2$  was controlled by biological respiration and microbial oxidation of organic matter ( $\delta^{13}\text{C}$  approximately -25‰ for C3 plants), and atmospheric  $\text{CO}_2$  ( $\delta^{13}\text{C}$  between -9 and -8‰), as suggested by Cerling et al. (1991) where low respiration rate leads to higher  $\delta^{13}\text{C}$  for soil  $\text{CO}_2$ . Moreover, the high values of  $\delta^{13}\text{C}$  in spring samples also may imply a significant degassing of  $\text{CO}_2$  from the springs before sampling (Deines et al., 1974).

The  $\delta^{13}\text{C}$  of selected spring samples behaves as predicted by models of calcite dissolution under open and closed system conditions if degassing is considered (Deines et al., 1974). However, in order to differentiate between closed and open system conditions the isotopic composition of the initial  $\text{CO}_2$  (soil  $\text{CO}_2$ ) has to be known because it represents the initial condition in the calculations.

### 3.2. Calculated $p\text{CO}_2$

The soil-rock  $p\text{CO}_2$  obtained by applying the inverse method

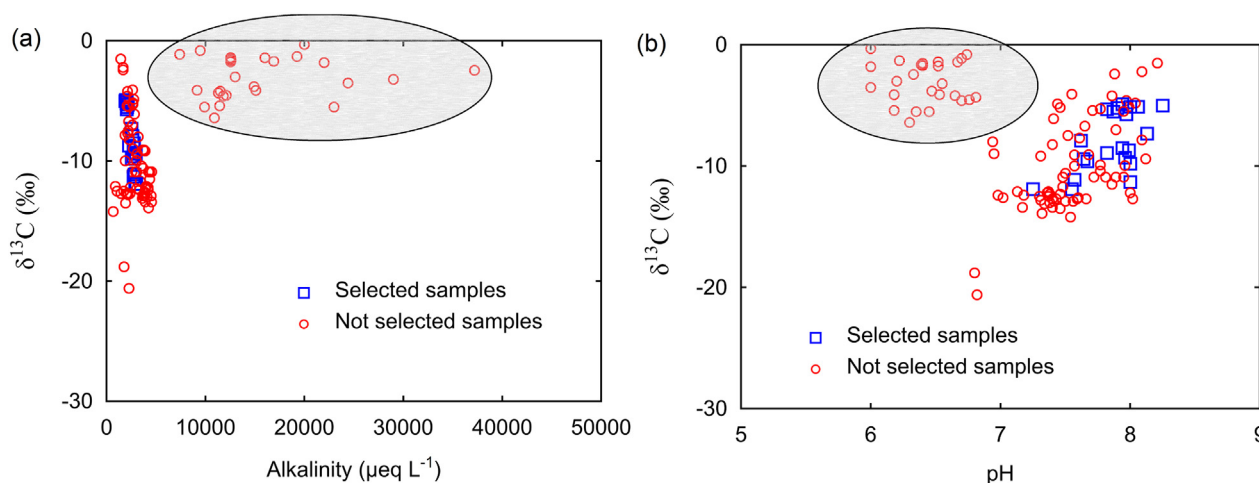


Fig. 4. Scatterplots for  $\delta^{13}\text{C}$  (‰) against (a) alkalinity ( $\mu\text{eq L}^{-1}$ ) and (b) pH. Selected spring samples based on Section 2.1 are represented by blue squares, red circles stand for the excluded sample points. The gray region shows samples with significant deep source of  $\text{CO}_2$ . (For interpretation of the references to colour in this figure legend, the reader is referred to the web version of this article.)

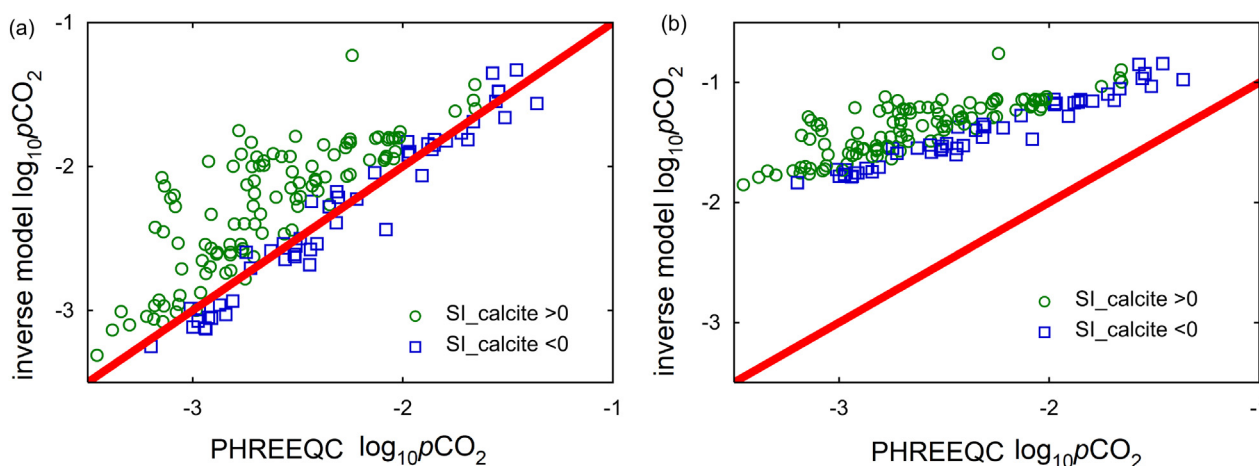


Fig. 5. Relation between calculated  $p\text{CO}_2$  applying the inverse method (Section 2.2) and water  $p\text{CO}_2$  calculated by PHREEQC software (PHREEQC  $\log_{10} p\text{CO}_2$ ) using 'Phreeqc.dat' database (Parkhurst and Appelo, 1999), for (a) open system condition and, (b) closed system condition. Red line represents the 1:1 relation. (For interpretation of the references to colour in this figure legend, the reader is referred to the web version of this article.)

(Section 2.2) is different from the spring water  $p\text{CO}_2$  (Fig. 5), calculated with PHREEQC using 'Phreeqc.dat' database and the equilibrium method (Parkhurst and Appelo, 1999). Spring water  $p\text{CO}_2$  represents the  $p\text{CO}_2$  at equilibrium with the pH and alkalinity of the spring water at the time the water sample was taken. The soil-rock  $p\text{CO}_2$  considering an open system condition is similar to the spring water  $p\text{CO}_2$  values (Fig. 5a). Oversaturated samples show higher soil-rock  $p\text{CO}_2$  values than spring water  $p\text{CO}_2$ , and undersaturated solutions plot on the 1:1 line (Fig. 5a) because the saturation index with respect calcite (SI) is near 0. When a closed system condition is considered, the soil-rock  $p\text{CO}_2$  values are much higher than the spring water  $p\text{CO}_2$  (Fig. 5b), but again oversaturated samples show on average elevated  $p\text{CO}_2$  values. These differences, based on the calcite saturation index (SI), are the result of considering equilibrium with calcite (SI of 0) in the soil-rock system with the inverse method (see method in Section 2.2). The available  $\delta^{13}\text{C}$  data may imply that degassing of  $\text{CO}_2$  in spring water is relevant in some cases (see discussion in Section 3.1). If degassing takes place, the calculated equilibrium  $p\text{CO}_2$  for the spring water decreases while increasing the saturation with respect to calcite. However, precipitation of calcite may not occur always immediately because the degassing rate of  $\text{CO}_2$  is significantly higher than the precipitation rate of calcite (Dreybrodt et al., 1996). Hence, the soil-rock  $p\text{CO}_2$  should be calculated applying the inverse method presented in this study

(considering SI = 0) using the chemical composition of spring samples rather than calculating the  $p\text{CO}_2$  at equilibrium with the spring water.

The soil-rock  $p\text{CO}_2$  under closed conditions ranges from 0.014 atm to 0.18 atm, and is thus clearly higher than open system conditions which range from 0.00049 atm to 0.059 atm (Fig. 6). The soil-rock  $p\text{CO}_2$  considering an open system fits in the range proposed by Yoshimura et al. (2001) for soil  $p\text{CO}_2$  for average Japanese soils (Fig. 6), unlike the closed system  $p\text{CO}_2$ , which shows even higher values than would be expected for humus soil conditions (Yoshimura et al., 2001). The closed condition presents high values of  $p\text{CO}_2$  at low temperature (near 3 °C); where less soil respiration is expected due to a decrease in biological activity. This implies that the underground production of  $\text{CO}_2$  related to  $\text{CaCO}_3\text{-H}_2\text{O-CO}_2$  system should lead to a partial pressure of approximately 0.01 atm, if a closed system is considered. However, the minimum value of  $p\text{CO}_2$  calculated considering an open system (0.00049 atm) is close to atmospheric  $p\text{CO}_2$ , which is comparable to results from respiration models (Cerling et al., 1991; Frisia et al., 2011; Lellei-Kovács et al., 2016; Suseela et al., 2012).

To further investigate the role of controlling variables on the calculated soil-rock  $p\text{CO}_2$ , a function (Eq. (10)) depending on temperature and soil volumetric water content ( $\theta$ ), variables commonly used in soil respiration models to explain soil respiration rates (Banerjee et al., 2016; Mielnick and Dugas, 2000), is fitted with the objective to

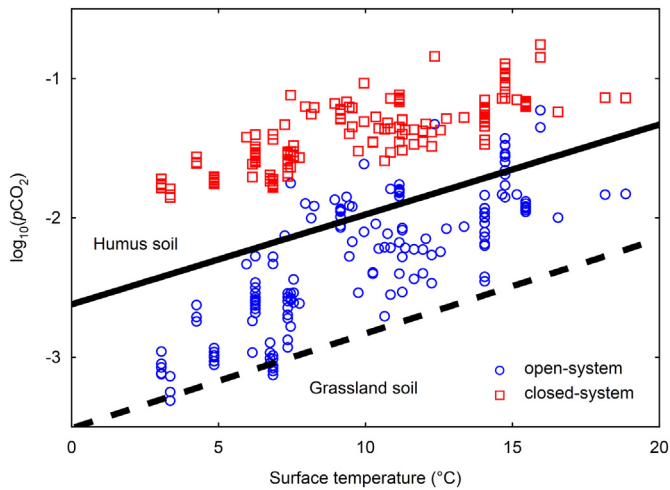


Fig. 6. Calculated partial pressure of  $\text{CO}_2$  against temperature with the introduced inverse method for open- (blue circles) and closed-system (red squares) conditions at equilibrium with calcite. Solid and dashed black lines are limits for soil  $p\text{CO}_2$  for average Japanese humus and grassland soils, respectively, taken from Yoshimura et al. (2001). The results for the closed system conditions are located above what would be expected for humus soil conditions. (For interpretation of the references to colour in this figure legend, the reader is referred to the web version of this article.)

introduce another dimension on the controls of soil-rock  $p\text{CO}_2$  for open system conditions. The dependency of soil respiration on soil volumetric water content is commonly represented as a polynomial function, presenting low respiration fluxes for both low and high values of soil volumetric water content. Soil respiration, generally, has maximum rates for soil volumetric water contents between  $0.2$  and  $0.4 \text{ m}^3 \text{ m}^{-3}$  (Banerjee et al., 2016; Ilstedt et al., 2000). In addition, temperature controls biological activity and thus influences soil  $p\text{CO}_2$ . Soil respiration is often described as being directly proportional to temperature (Lellei-Kovács et al., 2016; Lloyd and Taylor, 1994). Therefore, the

function developed to calculate the logarithm of the partial pressure of  $\text{CO}_2$  in the soil ( $\log_{10}p\text{CO}_2$ ) is represented by the following equation and based on findings from Fig. 7:

$$\log_{10} p\text{CO}_2 = \frac{e^{(b_1\theta) + \left(\frac{b_2}{\theta}\right)}}{(b_3 + e^{b_4T})} + \log_{10} p\text{CO}_{2\text{atm}} \quad (10)$$

where  $\theta$  represents the mean annual volumetric water content ( $v/v$ );  $T$  is the mean annual surface temperature in degrees Celsius,  $\log_{10}p\text{CO}_{2\text{atm}}$  is the logarithm of partial pressure of  $\text{CO}_2$  in the atmosphere (a value of  $-3.4$  was considered in this work);  $b_1$ ,  $b_2$ ,  $b_3$  and  $b_4$  are fitted constants with average values of  $-3.0 \pm 0.7$ ,  $-0.25 \pm 0.04$ ,  $0.09 \pm 0.03$  and  $-0.34 \pm 0.05$ , respectively. A random distribution of residuals is observed, indicating that the regression is not biased by the distribution of applied variables (Fig. 8). The standard deviation of the function calculated by residuals is  $\pm 0.3$  ( $\log_{10}p\text{CO}_2$ ), resulting in an interval of  $\pm 0.6$  ( $\log_{10}p\text{CO}_2$ ) for the 90% confidence level of the fitted function. The  $R^2$  between calculated soil-rock  $p\text{CO}_2$  by the inverse method and the estimated  $p\text{CO}_2$  by the fitted function is  $0.67$ , and thus significantly higher than the linear correlation between alkalinity and surface temperature with  $r^2 = 0.45$ , which does not consider soil volumetric water content.

The lower limit in Eq. (10) is considered to be the  $p\text{CO}_2$  concentration in the atmosphere, where soil respiration is low and atmospheric  $\text{CO}_2$  diffuses from the atmosphere into the soil (Dörr and Münich, 1980). Furthermore, a maximum threshold for soil  $p\text{CO}_2$  is established based on the spring water chemistry, which may represent the limit of biological activity. However, it is not possible to predict  $p\text{CO}_2$  at higher land temperatures ( $> 20^\circ\text{C}$ ) due to the absence of data. Therefore, global applications might be limited by the range of temperature ( $3$  to  $19^\circ\text{C}$ ) and soil volumetric water content (from  $0.17$  to  $0.37 \text{ m}^3 \text{ m}^{-3}$ ) in the applied dataset for the development of the function. The function may also be only applicable for catchments dominated by carbonate rocks, until further studies confirm the identified pattern.

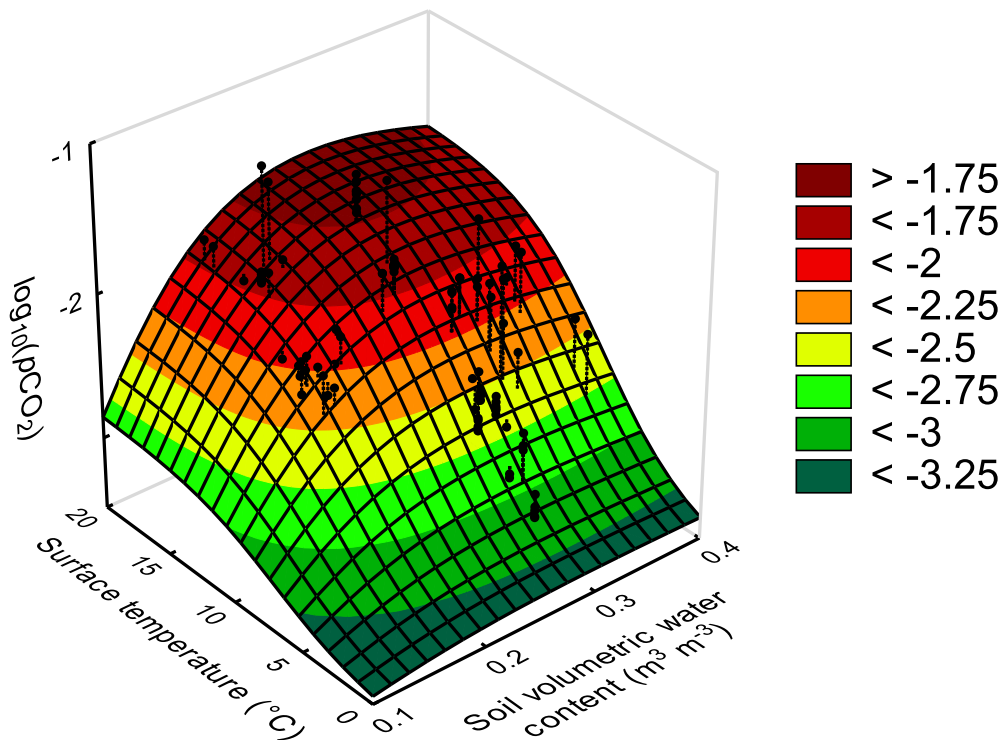


Fig. 7. Fitted function representing the soil  $p\text{CO}_2$  (Eq. (10)) depending on mean annual surface temperature ( $^\circ\text{C}$ ) and mean annual volumetric water content ( $\text{m}^3 \text{ m}^{-3}$ ). Black points represent the calculated  $p\text{CO}_2$  based on the inverse method (Section 2.2). Coloured regions represent different values of  $\log_{10}p\text{CO}_2$ .

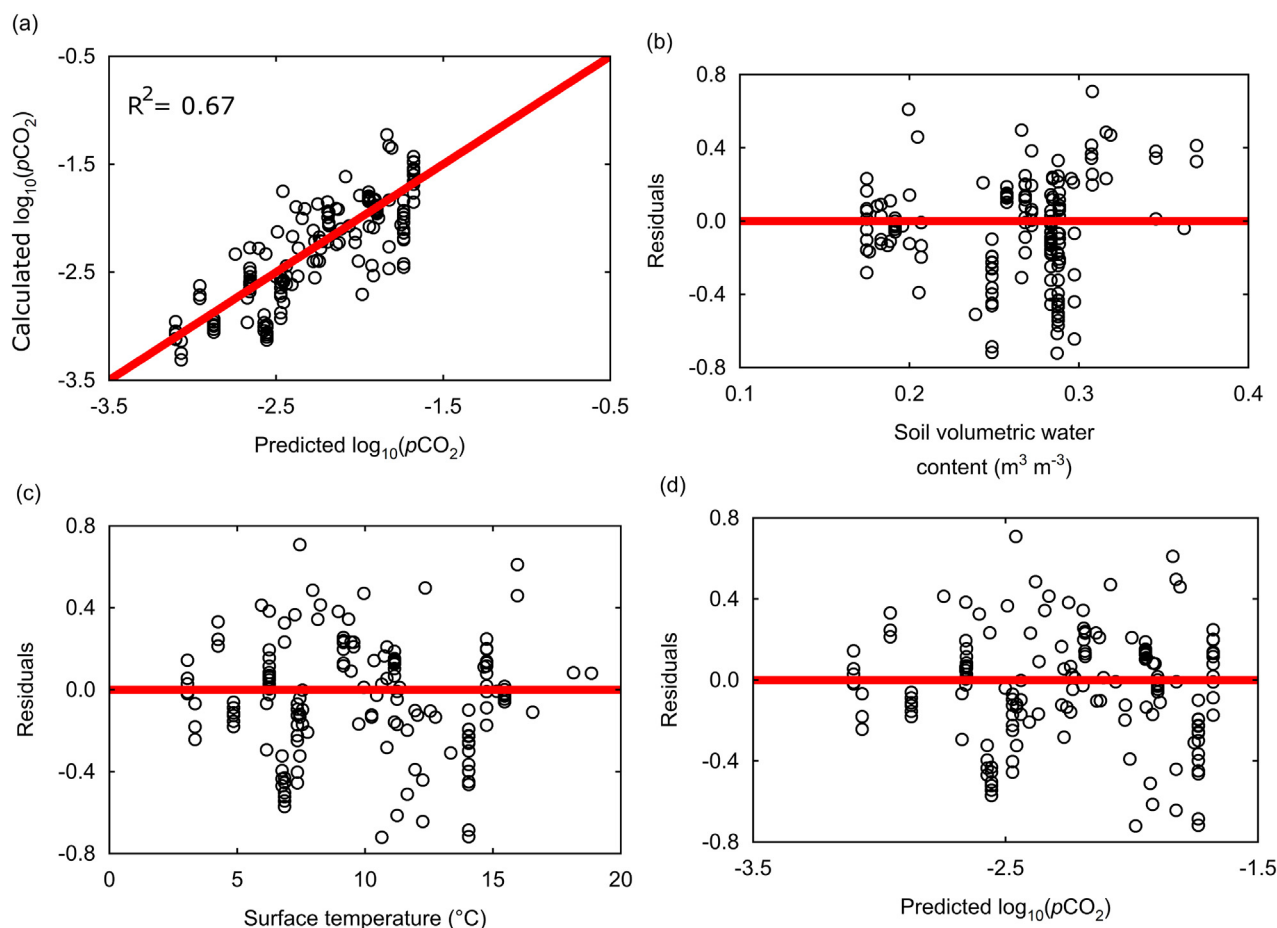


Fig. 8. Predicted  $p\text{CO}_2$  against calculated  $p\text{CO}_2$  values and residuals plots for the new parameterization of  $p\text{CO}_2$  (Eq. (10)). (a) Calculated  $p\text{CO}_2$  against predicted  $p\text{CO}_2$  values, (b) residuals against soil volumetric water content, (c) residuals against surface temperature, and (d) residuals against predicted  $p\text{CO}_2$  values. The red line represents the condition in which residuals are equal to zero. The partial pressures of  $\text{CO}_2$  are expressed as decimal logarithm of atmosphere. Residuals were calculated as: Observed values – Predicted values. (For interpretation of the references to colour in this figure legend, the reader is referred to the web version of this article.)

#### 4. Discussion

This work shows that spring water samples can be used to estimate an average soil-rock  $p\text{CO}_2$ , considering open system conditions. The proposed model-framework can be used to estimate alkalinity fluxes out of the soil-rock system using climate relevant parameters like temperature and soil water content, which are forcing factors on soil respiration rates and thus  $\text{CO}_2$  production. With this it is possible to link alkalinity exported from a soil-rock system into a river system with climate forcing. This framework can be improved if more data from climate regions are included, for which now a gap exist.

Data selection was an imperative step in order to apply the presented inverse soil-rock  $p\text{CO}_2$  calculation method. For instance, relevant dissolution of evaporite, sulfide and silicate minerals would result into different values as estimated based on an ideal calcium carbonate system with respect to alkalinity concentrations and  $\text{CO}_2$ -consumption. In a system at equilibrium with gypsum, calcite, water and  $\text{CO}_2$  the alkalinity concentrations are approximately 40% lower than in a pure calcite-water- $\text{CO}_2$  system (Fig. 9), because of the common ion effect, where  $\text{Ca}^{2+}$  concentration depends on dissolution of both minerals. The presented analysis framework can, however, be enhanced by further relevant processes or above named mineral groups, which influence the alkalinity production, if sufficient constraints can be implemented. But this demands that the sources of sulfate (gypsum versus sulfide) need to be known to account for the different effects of both mineral groups (sulfur isotopes are one measure to achieve this). In addition,  $\delta^{13}\text{C}$  isotope data can be employed to constrain processes like degassing,

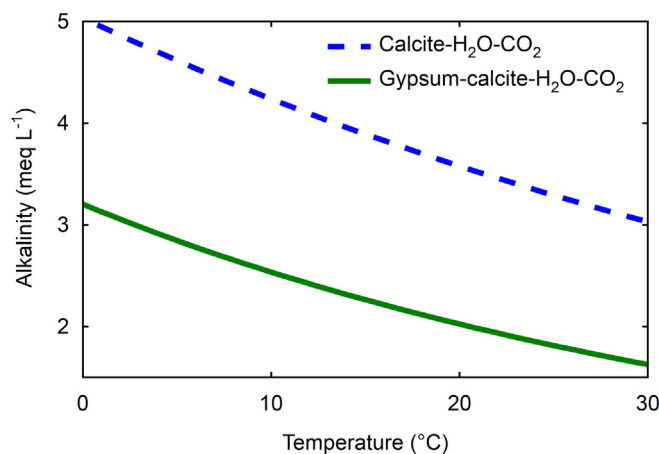
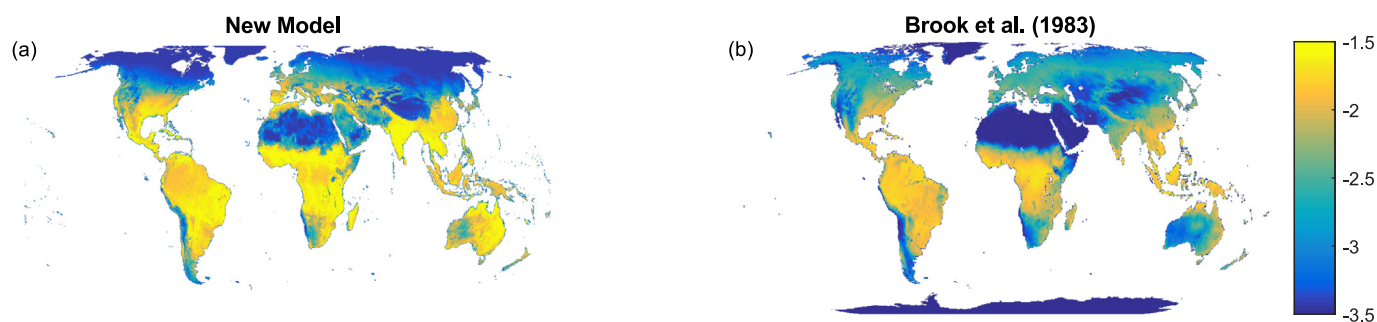


Fig. 9. Alkalinity against temperature for calcite- $\text{H}_2\text{O}$ - $\text{CO}_2$  (blue dash line) and gypsum-calcite- $\text{H}_2\text{O}$ - $\text{CO}_2$  (green line) systems at constant  $\log_{10}p\text{CO}_2$  value of  $-2$ . Results were obtained using the software PHREEQC with 'Phreeqc.dat' database (Parkhurst and Appelo, 1999). (For interpretation of the references to colour in this figure legend, the reader is referred to the web version of this article.)

contribution of deep  $\text{CO}_2$  sources, or the role of ecosystem composition and its contribution to the  $\text{CO}_2$ -budget.

The spring water chemistry in karst regions may be developed under different system conditions (open, closed and semi-open conditions) and with influence of different  $\text{CO}_2$  sources (Fig. 4). However, results



**Fig. 10.** Comparison of global soil  $p\text{CO}_2$  maps using two different equations: (a) this study, using Eq. (10) based on temperature and soil water content for open system conditions, and (b) Eq. (11) based on actual annual evapotranspiration (Brook et al., 1983). Colour bar shows  $\log_{10}p\text{CO}_2$  values. Value ranges of applied data for deriving functions for predicted soil-rock  $p\text{CO}_2$  should limit the application area. Appendix A shows the areas which have value ranges for land surface temperature and soil volumetric water content within the ranges of the dataset used in Eq. (10).

based on the filtered data suggest a dominance of open system conditions (Fig. 6). However, previous studies have found spring water samples from karstic areas which might have developed under semi-open system conditions (Calmels et al., 2014; Geldern et al., 2015).

#### 4.1. Parameterization for estimating soil-rock $p\text{CO}_2$

The dissolution of soil-rock  $\text{CO}_2$  into water was considered to be the only hydronium ion contributor for carbonate weathering reactions in the presented analysis framework, without taking into account the contribution of organic acids to the acidification of soils, relevant in organic-rich soils (Thorley et al., 2015). However, soil biological activity promotes  $\text{CO}_2$  respiration and hence chemical weathering caused by carbonic acid. In addition, in the soil system, without considering organic acids, the rate-determining process of carbonate weathering is the dissolution of  $\text{CO}_2$  in water, which is regulated by the action of the carbonic anhydrase (CA) enzyme in soils (Liu et al., 2005). Furthermore, carbonate weathering can be enhanced by reacting with sulfuric acid. This acid may be produced naturally by the oxidation of sulfide minerals, or related to anthropogenic sources (Beaulieu et al., 2011; Li et al., 2008; Torres et al., 2014; Wang et al., 2015).

Temperature and soil volumetric water content are parameters characteristic of climate conditions, because they play an important role in the budgets of land energy and water balance (Seneviratne et al., 2010). Additionally, the increase in the volumetric water content directly affects microbial activity in the soil, while reducing gaseous and liquid diffusion rates and limiting the supply of oxygen and other gases (Banerjee et al., 2016; Blagodatsky and Smith, 2012). On the other hand, lower values of soil volumetric water content limit the growth rate of plants and the biological activity in the soil (Ilstedt et al., 2000). These conditions explain the shape of the estimated soil-rock  $p\text{CO}_2$  by using land surface temperature and soil water content as predictors for open system conditions (Fig. 7), exhibiting a maximum  $p\text{CO}_2$  value in soils with volumetric water content between  $0.2$  and  $0.4 \text{ m}^3 \text{ m}^{-3}$ . The relatively good correlation of soil-rock  $p\text{CO}_2$  solely with temperature (Fig. 6) demonstrates that soil-rock  $p\text{CO}_2$  is highly sensitive to climate variability. Thus, it is possible to estimate the soil-rock  $p\text{CO}_2$  only by temperature, when water availability is not a limiting variable, as found by Schwendenmann and Veldkamp (2006) in tropical forests, where the  $\text{CO}_2$  was highly correlated with temperature. The compilation used in this work misses values for low and high water contents and high annual land temperatures (higher than  $20^\circ\text{C}$ ), and it remains therefore unclear if with new data the  $p\text{CO}_2$  function based on water content and temperature would result in different  $p\text{CO}_2$  values than calculated here.

The soil-rock  $p\text{CO}_2$  calculated in this work is representative of depths where weathering reactions occur in carbonate lithologies, because it was calculated after applying a data filtering in order to exclude

spring samples under the influence of  $\text{CO}_2$  from deep sources and hydrothermal processes. Therefore, the soil-rock  $p\text{CO}_2$  functions presented in this work represent the  $p\text{CO}_2$  of interest for weathering reactions comparable to other functions such as the one reported by Brook et al. (1983), in which the soil  $\text{CO}_2$  at different depths was correlated with actual annual evapotranspiration (AET) and atmospheric  $p\text{CO}_2$  ( $p\text{CO}_2\text{atm}$ ) by the following equation:

$$\log_{10}(p\text{CO}_2) = \log_{10}(p\text{CO}_2\text{atm}) + 2.09(1 - e^{-0.00172\text{AET}}) \quad (11)$$

As there exist not many approaches to estimate global patterns of soil  $p\text{CO}_2$ , the values derived from this work based on Eq. (10) are compared for a plausibility test with results obtained using the equation presented by Brook et al. (1983). Global data for AET and annual water content was taken from the Global Land Evaporation Amsterdam Model (GLEAMv3.0). This model consists of a set of algorithms that calculate the different components of terrestrial hydrological water cycle based on satellite observations (Martens et al., 2016; Miralles et al., 2011). Results obtained applying Eq. (10) based on this work shows the imprint of temperature and soil water content. For cold regions, low soil  $p\text{CO}_2$  are predicted while some humid areas close to the equator show highest soil  $p\text{CO}_2$  values (Fig. 10a). Soil  $p\text{CO}_2$  in arid areas are lower than in humid tropical areas due to low water content values. The soil  $p\text{CO}_2$  map obtained using Eq. (11) after Brook et al. (1983) with AET as predictor (Fig. 10b) shows a similar spatial pattern as results from Eq. (10). However, differences are observed in low temperature regions and deserts. The Brook et al. (1983) function was created comparing mean annual values of actual annual evapotranspiration with soil  $\text{CO}_2$  measured during the growing seasons. This implies that in low temperature regions Eq. (11) may overestimate the real mean annual values. Frisia et al. (2011) found that soil  $p\text{CO}_2$  from the *Grotta di Ernesto* region, classified as mesothermic-humid climate, can decrease significantly during the winter season ( $< 5^\circ\text{C}$ ) reaching values close to atmospheric  $p\text{CO}_2$ . This behaviour is not represented by Eq. (11). Despite the general good agreement in the patterns and ranges of  $p\text{CO}_2$  at the global scale, the formulation of Eq. (10) may be a better approach for parameterization of the mean annual soil  $\text{CO}_2$  in cold regions, and it can be applied not only to represent mean annual values but to represent seasonal changes, because it will follow temperature changes and water content changes. The simple formulation for a soil  $p\text{CO}_2$  function allows constraining the  $p\text{CO}_2$  by climate variables without the need of a complex ecosystem model, which has advantages for the study of changes at the global scale over longer time scales for which such a function is representative.

#### 4.2. Global applications

The difference in carbonate rock-soil  $p\text{CO}_2$  is mainly influenced by



the biological activity in the soil system, which in turn depends on the temperature and water availability. As a result, the  $p\text{CO}_2$  estimation framework developed in this work may be a good predictor for soil-rock  $p\text{CO}_2$  at a global scale for carbonate rock systems, and possible for other systems in general. Nevertheless, the available data should be enhanced by data from karst areas in high and low temperature regions, and regions with extreme conditions for soil volumetric water content, to ascertain a valid global application (Appendix A, Fig. A.1). If the framework holds for non-carbonate rock conditions, it might be applicable to a much wider range of land areas in general. It should also be considered to enhance the model framework by further factors, which are relevant for weathering products from carbonate sedimentary rocks in general, namely evaporite, sulfide and silicate minerals.

The present framework produces a soil-rock  $p\text{CO}_2$ , which is comparable in its dependency of temperature and soil water content as implemented in soil respiration flux models, and mechanistically consistent with complex ecosystem functioning. An implementation into global weathering models would allow to represent ecosystem functioning, but would not demand the computational power of incorporating explicit results from complex ecosystem models.

In this way, it might be possible to improve current phenomenological global weathering models in order to consider the soil-rock partial pressure of  $\text{CO}_2$  as an important constraint, because it represents a major source of acidity to the water-soil-rock system and its concentration depends on climate conditions. In parallel to the implementation of the new parameterization for soil-rock  $p\text{CO}_2$  into global weathering models, results should be compared with measurements of  $\text{CO}_2$  in the soil-rock system under a wide range of temperature and soil water content conditions.

## 5. Conclusions

The chemistry of spring waters in areas dominated by carbonate

## Appendix A. Temperature and soil water content ranges

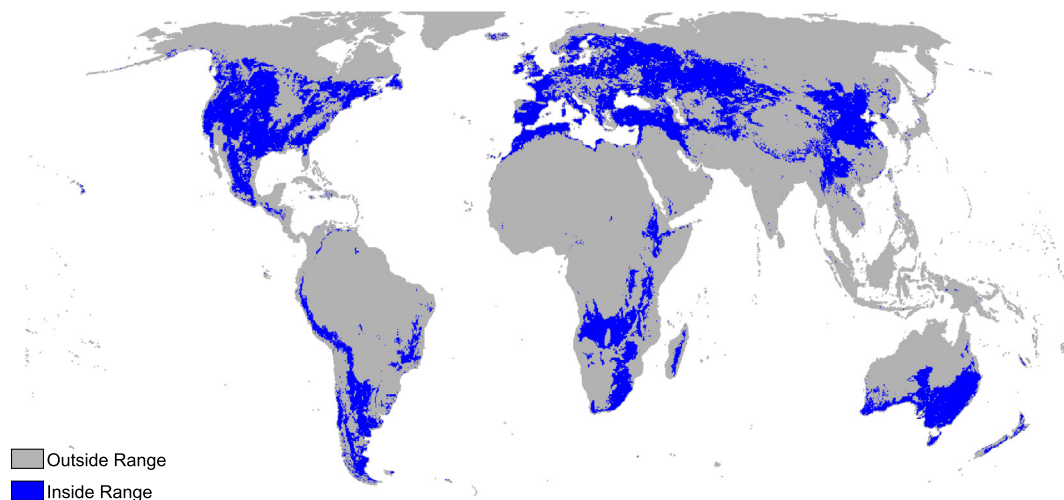


Fig. A.1. Distribution of areas within the range of land temperature (0.4 to 22.0 °C) and soil water content (0.17 to 0.37  $\text{m}^{-3} \text{m}^{-3}$ ) of the 164 selected spring samples. Blue indicates the regions with the same range and in gray are the regions with different land temperature or soil water content.

## References

- Abongwa, P.T., Atekwana, E.A., 2015. Controls on the chemical and isotopic composition of carbonate springs during evolution to saturation with respect to calcite. *Chem. Geol.* 404, 136–149.
- Amundson, R.G., Davidson, E.A., 1990. Carbon dioxide and nitrogenous gases in the soil atmosphere. *J. Geochem. Explor.* 38 (1), 13–41.
- Banerjee, S., Helgason, B., Wang, L., Winsley, T., Ferrari, B.C., Siciliano, S.D., 2016.

rocks retains a climate and ecosystem signature, suggesting dissolution of minerals under open system conditions with respect to soil-rock  $\text{CO}_2$ . Therefore, the chemistry of spring waters from catchments dominated by calcium carbonate rocks can be used to estimate the soil-rock  $p\text{CO}_2$ .

The parameterization for a soil-rock  $p\text{CO}_2$  represents an averaged condition of the catchment of the spring waters, and it is centered on model behaviour for soil respiration fluxes. The approach can be employed in studies aimed to quantify calcite weathering fluxes from the terrestrial system into the fluvial system. The presented framework could be enhanced for global scale application to reproduce common settings including dolomite, evaporite and sulfide weathering processes, if additional data sources are compiled and available. As current phenomenological models for prediction of global carbonate weathering do not consider soil  $p\text{CO}_2$  as a constraining variable, new approaches may consider soil-rock  $p\text{CO}_2$  forced by climate sensitive variables to better understand the control of climate change on carbonate weathering.

Supplementary data to this article can be found online at <https://doi.org/10.1016/j.chemgeo.2018.01.030>.

## Acknowledgments

Funding for this work has been provided by German Research Foundation (DFG) through the Cluster of Excellence CLISAP2 (DFG Exec177, Universität Hamburg), and BMBF-project PALMOD (Ref 01LP1506C) through the German Federal Ministry of Education and Research (BMBF) as Research for Sustainability initiative (FONA). The authors thank the two anonymous reviewers and the editor constructive comments. We further thank M.Sc. Felix Amoako Boampong for his help provided during data acquisition.

- Legacy effects of soil moisture on microbial community structure and  $\text{N}_2\text{O}$  emissions. *Soil Biol. Biochem.* 95, 40–50.
- Beaulieu, E., Godd eris, Y., Labat, D., Roelandt, C., Calmels, D., Gaillardet, J., 2011. Modeling of water-rock interaction in the Mackenzie basin: competition between sulfuric and carbonic acids. *Chem. Geol.* 289 (1), 114–123.
- Beaulieu, E., Godd eris, Y., Donnadi eu, Y., Labat, D., Roelandt, C., 2012. High sensitivity of the continental-weathering carbon dioxide sink to future climate change. *Nat. Clim. Chang.* 2 (5), 346–349.
- Berner, R.A., Lasaga, A.C., Garrels, R.M., 1983. The carbonate-silicate geochemical cycle

- and its effect on atmospheric carbon dioxide over the past 100 million years. *Am. J. Sci.* 283, 641–683.
- Blagodatsky, S., Smith, P., 2012. Soil physics meets soil biology: towards better mechanistic prediction of greenhouse gas emissions from soil. *Soil Biol. Biochem.* 47, 78–92.
- Bluth, G.J., Kump, L.R., 1994. Lithologic and climatologic controls of river chemistry. *Geochim. Cosmochim. Acta* 58 (10), 2341–2359.
- Brook, G.A., Folkoff, M.E., Box, E.O., 1983. A world model of soil carbon dioxide. *Earth Surf. Process. Landf.* 8 (1), 79–88.
- Calmels, D., Gaillardet, J., François, L., 2014. Sensitivity of carbonate weathering to soil CO<sub>2</sub> production by biological activity along a temperate climate transect. *Chem. Geol.* 390, 74–86.
- Cartwright, J., Hui, D., 2014. Soil respiration patterns and controls in limestone cedar glades. *Plant Soil* 389 (1–2), 157–169.
- Cerling, T.E., Solomon, D.K., Quade, J., Bowman, J.R., 1991. On the isotopic composition of carbon in soil carbon dioxide. *Geochim. Cosmochim. Acta* 55 (11), 3403–3405.
- Chiodini, G., Frondini, F., Kerrick, D., Rogie, J., Parello, F., Peruzzi, L., Zanzari, A., 1999. Quantification of deep CO<sub>2</sub> fluxes from Central Italy. Examples of carbon balance for regional aquifers and of soil diffuse degassing. *Chem. Geol.* 159 (1), 205–222.
- Dandurand, J., Gout, R., Hoefs, J., Menschel, G., Schott, J., Usdowski, E., 1982. Kinetically controlled variations of major components and carbon and oxygen isotopes in a calcite-precipitating spring. *Chem. Geol.* 36 (3–4), 299–315.
- Deines, P., Langmuir, D., Harmon, R.S., 1974. Stable carbon isotope ratios and the existence of a gas phase in the evolution of carbonate ground waters. *Geochim. Cosmochim. Acta* 38 (7), 1147–1164.
- Dorigo, W.A., Gruber, A., De Jeu, R.A.M., Wagner, W., Stacke, T., Loew, A., Albergel, C., Brocca, L., Chung, D., Parinussa, R.M., Kidd, R., 2015. Evaluation of the ESA CCI soil moisture product using ground-based observations. *Remote Sens. Environ.* 162, 380–395.
- Dörr, H., Münnich, K.O., 1980. Carbon-14 and carbon-13 in soil CO<sub>2</sub>. *Radiocarbon* 22 (03), 909–918.
- Dreybrodt, W., Lauckner, J., Zaihua, L., Svensson, U., Buhmann, D., 1996. The kinetics of the reaction CO<sub>2</sub> + H<sub>2</sub>O → H<sup>+</sup> + HCO<sub>3</sub><sup>-</sup> as one of the rate limiting steps for the dissolution of calcite in the system H<sub>2</sub>O–CO<sub>2</sub>–CaCO<sub>3</sub>. *Geochim. Cosmochim. Acta* 60 (18), 3375–3381.
- Epron, D., Farque, L., Lucot, É., Badot, P.-M., 1999. Soil CO<sub>2</sub> efflux in a beech forest: dependence on soil temperature and soil water content. *Ann. For. Sci.* 56 (3), 221–226.
- Frisia, S., Fairchild, L.J., Fohlmeister, J., Miorandi, R., Spötl, C., Borsato, A., 2011. Carbon mass-balance modelling and carbon isotope exchange processes in dynamic caves. *Geochim. Cosmochim. Acta* 75 (2), 380–400.
- Gaillardet, J., Dupré, B., Louvat, P., Allegre, C., 1999. Global silicate weathering and CO<sub>2</sub> consumption rates deduced from the chemistry of large rivers. *Chem. Geol.* 159 (1), 3–30.
- Gaumont-Guay, D., Black, T.A., Griffis, T.J., Barr, A.G., Jassal, R.S., Nescic, Z., 2006. Interpreting the dependence of soil respiration on soil temperature and water content in a boreal aspen stand. *Agric. For. Meteorol.* 140 (1), 220–235.
- Geldern, R., Schulte, P., Mader, M., Baier, A., Barth, J.A., 2015. Spatial and temporal variations of pCO<sub>2</sub>, dissolved inorganic carbon and stable isotopes along a temperate karstic watercourse. *Hydrol. Process.* 29 (15), 3423–3440.
- Goddéris, Y., François, L.M., Probst, A., Schott, J., Moncoulon, D., Labat, D., Viville, D., 2006. Modelling weathering processes at the catchment scale: the WITCH numerical model. *Geochim. Cosmochim. Acta* 70 (5), 1128–1147.
- Goddéris, Y., Brantley, S.L., François, L.M., Schott, J., Pollard, D., Déqué, M., Dury, M., 2013. Rates of consumption of atmospheric CO<sub>2</sub> through the weathering of loess during the next 100 yr of climate change. *Biogeosciences* 10 (1), 135–148.
- Goll, D.S., Moosdorf, N., Hartmann, J., Brovkin, V., 2014. Climate-driven changes in chemical weathering and associated phosphorus release since 1850: implications for the land carbon balance. *Geophys. Res. Lett.* 41 (10), 3553–3558.
- Hartmann, J., 2009. Bicarbonate-fluxes and CO<sub>2</sub>-consumption by chemical weathering on the Japanese Archipelago - application of a multi-lithological model framework. *Chem. Geol.* 265 (3–4), 237–271.
- Hartmann, J., Jansen, N., Durr, H.H., Kempe, S., Kohler, P., 2009. Global CO<sub>2</sub>-consumption by chemical weathering: what is the contribution of highly active weathering regions? *Glob. Planet. Chang.* 69 (4), 185–194.
- Hartmann, J., Moosdorf, N., Lauerwald, R., Hinderer, M., West, A.J., 2014. Global chemical weathering and associated P-release — the role of lithology, temperature and soil properties. *Chem. Geol.* 363, 145–163.
- Herman, J.S., Lorah, M.M., 1987. CO<sub>2</sub> outgassing and calcite precipitation in Falling Spring Creek, Virginia, USA. *Chem. Geol.* 62 (3–4), 251–262.
- Hijmans, R.J., Cameron, S.E., Parra, J.L., Jones, P.G., Jarvis, A., 2005. Very high resolution interpolated climate surfaces for global land areas. *Int. J. Climatol.* 25 (15), 1965–1978.
- Huang, F., Zhang, C., Xie, Y., Li, L., Cao, J., 2015. Inorganic carbon flux and its source in the karst catchment of Maocun, Guilin, China. *Environ. Earth Sci.* 74 (2), 1079–1089.
- Ilstedt, U., Nordgren, A., Malmer, A., 2000. Optimum soil water for soil respiration before and after amendment with glucose in humid tropical Acrisols and a boreal mor layer. *Soil Biol. Biochem.* 32 (11), 1591–1599.
- Jacobson, R.L., Langmuir, D., 1970. The chemical history of some spring waters in carbonate rocks. *Ground Water* 8 (3), 5–9.
- Jacobson, R.L., Langmuir, D., 1974. Controls on the quality variations of some carbonate spring waters. *J. Hydrol.* 23 (3–4), 247–265.
- Jeelani, G., Bhat, N.A., Shivanna, K., Bhat, M., 2011. Geochemical characterization of surface water and spring water in SE Kashmir Valley, western Himalaya: implications to water–rock interaction. *J. Earth Syst. Sci.* 120 (5), 921–932.
- Kanduč, T., Mori, N., Kocman, D., Stibilj, V., Grassa, F., 2012. Hydrogeochemistry of Alpine springs from North Slovenia: insights from stable isotopes. *Chem. Geol.* 300–301, 40–54.
- Karimi, H., Raeisi, E., Bakalowicz, M., 2005. Characterising the main karst aquifers of the Alvand basin, northwest of Zagros, Iran, by a hydrogeochemical approach. *Hydrogeol. J.* 13 (5–6), 787–799.
- Kohfahl, C., Sprenger, C., Herrera, J.B., Meyer, H., Chacon, F.F., Pekdeger, A., 2008. Recharge sources and hydrogeochemical evolution of groundwater in semiarid and karstic environments: a field study in the Granada Basin (Southern Spain). *Appl. Geochem.* 23 (4), 846–862.
- Kuzyakov, Y., 2006. Sources of CO<sub>2</sub> efflux from soil and review of partitioning methods. *Soil Biol. Biochem.* 38 (3), 425–448.
- Langmuir, D., 1971. The geochemistry of some carbonate ground waters in central Pennsylvania. *Geochim. Cosmochim. Acta* 35 (10), 1023–1045.
- Lellei-Kovács, E., Botta-Dukát, Z., de Dato, G., Estiarte, M., Guidolotti, G., Kopittke, G.R., Kovács-Láng, E., Kröel-Dulay, G., Larsen, K.S., Peñuelas, J., Smith, A.R., Sowerby, A., Tietema, A., Schmidt, I.K., 2016. Temperature dependence of soil respiration modulated by thresholds in soil water availability across European shrubland ecosystems. *Ecosystems* 19 (8), 1460–1477.
- Li, S.-L., Calmels, D., Han, G., Gaillardet, J., Liu, C.-Q., 2008. Sulfuric acid as an agent of carbonate weathering constrained by δ<sup>34</sup>S<sub>CDIC</sub>: examples from Southwest China. *Earth Planet. Sci. Lett.* 270 (3–4), 189–199.
- Liu, Z., Yuan, D., Dreybrodt, W., 2005. Comparative study of dissolution rate-determining mechanisms of limestone and dolomite. *Environ. Geol.* 49 (2), 274–279.
- Liu, Y., Dorigo, W.A., Parinussa, R., de Jeu, R.A., Wagner, W., McCabe, M.F., Evans, J., Van Dijk, A., 2012. Trend-preserving blending of passive and active microwave soil moisture retrievals. *Remote Sens. Environ.* 123, 280–297.
- Lloyd, J., Taylor, J., 1994. On the temperature dependence of soil respiration. *Funct. Ecol.* 315–323.
- Long, X., Sun, Z., Zhou, A., Liu, D., 2015. Hydrogeochemical and isotopic evidence for flow paths of karst waters collected in the Heshang Cave, Central China. *J. Earth Sci.* 26 (1), 149–156.
- Lopez-Chicano, M., Bouamama, M., Vallejos, A., Pulido-Bosch, A., 2001. Factors which determine the hydrogeochemical behaviour of karstic springs. A case study from the Betic Cordilleras, Spain. *Appl. Geochem.* 16 (9), 1179–1192.
- Martens, B., Miralles, D.G., Lievens, H., van der Schalie, R., de Jeu, R.A., Fernández-Prieto, D., Beck, H.E., Dorigo, W.A., Verhoest, N.E., 2016. GLEAM v3: satellite-based land evaporation and root-zone soil moisture. *Geosci. Model Dev. Discuss.* 1–36.
- Mielnick, P., Dugas, W.A., 2000. Soil CO<sub>2</sub> flux in a tallgrass prairie. *Soil Biol. Biochem.* 32 (2), 221–228.
- Miralles, D., Holmes, T., De Jeu, R., Gash, J., Meesters, A., Dolman, A., 2011. Global land-surface evaporation estimated from satellite-based observations. *Hydrol. Earth Syst. Sci.* 15 (2), 453.
- Moral, F., Cruz-Sanjulián, J.J., Olías, M., 2008. Geochemical evolution of groundwater in the carbonate aquifers of Sierra de Segura (Betic Cordillera, southern Spain). *J. Hydrol.* 360 (1–4), 281–296.
- Özkul, M., Gökgöz, A., Horvatinčić, N., 2010. Depositional properties and geochemistry of Holocene perched springline tufa deposits and associated spring waters: a case study from the Denizli Province, Western Turkey. *Geol. Soc. Lond., Spec. Publ.* 336 (1), 245–262.
- Parkhurst, D.L., Appelo, C., 1999. User's Guide to PHREEQC (Version 2): A Computer Program for Speciation, Batch-reaction, One-dimensional Transport, and Inverse Geochemical Calculations.
- Pu, T., He, Y., Zhang, T., Wu, J., Zhu, G., Chang, L., 2013. Isotopic and geochemical evolution of ground and river waters in a karst dominated geological setting: a case study from Lijiang basin, South-Asia monsoon region. *Appl. Geochem.* 33, 199–212.
- Qibo, H., Xiaoqun, Q., Qiyong, Y., Pengyu, L., Jinsong, Z., 2016. Identification of dissolved sulfate sources and the role of sulfuric acid in carbonate weathering using δ<sup>13</sup>C<sub>CDIC</sub> and δ<sup>34</sup>S in karst area, northern China. *Environ. Earth Sci.* 75 (1).
- Raich, J.W., Potter, C.S., 1995. Global patterns of carbon dioxide emissions from soils. *Glob. Biogeochem. Cycles* 9 (1), 23–36.
- Reddy, M.M., Plummer, L.N., Busenberg, E., 1981. Crystal growth of calcite from calcium bicarbonate solutions at constant P CO<sub>2</sub> and 25 °C: a test of a calcite dissolution model. *Geochim. Cosmochim. Acta* 45 (8), 1281–1289.
- Roelandt, C., Goddéris, Y., Bonnet, M.P., Sondag, F., 2010. Coupled modeling of biogeochemical and chemical weathering processes at the continental scale. *Glob. Biogeochem. Cycles* 24 (2) (n/a–n/a).
- Roland, M., Serrano-Ortiz, P., Kowalski, A.S., Goddéris, Y., Sánchez-Cañete, E.P., Ciais, P., Domingo, F., Cuezva, S., Sanchez-Moral, S., Longdoz, B., Yakir, D., Van Grieken, R., Schott, J., Cardell, C., Janssens, I.A., 2013. Atmospheric turbulence triggers pronounced diel pattern in karst carbonate geochemistry. *Biogeosciences* 10 (7), 5009–5017.
- Schwendenmann, L., Veldkamp, E., 2006. Long-term CO<sub>2</sub> production from deeply weathered soils of a tropical rain forest: evidence for a potential positive feedback to climate warming. *Glob. Chang. Biol.* 12 (10), 1878–1893.
- Seneviratne, S.I., Corti, T., Davin, E.L., Hirschi, M., Jaeger, E.B., Lehner, I., Orlowsky, B., Teuling, A.J., 2010. Investigating soil moisture–climate interactions in a changing climate: a review. *Earth Sci. Rev.* 99 (3–4), 125–161.
- Serrano-Ortiz, P., Roland, M., Sanchez-Moral, S., Janssens, I.A., Domingo, F., Goddéris, Y., Kowalski, A.S., 2010. Hidden, abiotic CO<sub>2</sub> flows and gaseous reservoirs in the terrestrial carbon cycle: review and perspectives. *Agric. For. Meteorol.* 150 (3), 321–329.
- Smith, H., Wood, P., 2002. Flow permanence and macroinvertebrate community variability in limestone spring systems. *Hydrobiologia* 487 (1), 45–58.
- Suchet, P.A., Probst, J.-L., 1993. Modelling of atmospheric CO<sub>2</sub> consumption by chemical weathering of rocks: application to the Garonne, Congo and Amazon basins. *Chem. Geol.* 107 (3), 205–210.

- Suseela, V., Conant, R.T., Wallenstein, M.D., Dukes, J.S., 2012. Effects of soil moisture on the temperature sensitivity of heterotrophic respiration vary seasonally in an old-field climate change experiment. *Glob. Chang. Biol.* 18 (1), 336–348.
- Szramek, K., Walter, L.M., 2004. Impact of carbonate precipitation on riverine inorganic carbon mass transport from a mid-continent, forested watershed. *Aquat. Geochem.* 10 (1), 99–137.
- Szramek, K., Walter, L.M., Kanduč, T., Ogrinc, N., 2011. Dolomite versus calcite weathering in hydrogeochemically diverse watersheds established on bedded carbonates (Sava and Soča Rivers, Slovenia). *Aquat. Geochem.* 17 (4–5), 357–396.
- Thorley, R.M., Taylor, L.L., Banwart, S.A., Leake, J.R., Beerling, D.J., 2015. The role of forest trees and their mycorrhizal fungi in carbonate rock weathering and its significance for global carbon cycling. *Plant Cell Environ.* 38 (9), 1947–1961.
- Torres, M.A., West, A.J., Li, G., 2014. Sulphide oxidation and carbonate dissolution as a source of CO<sub>2</sub> over geological timescales. *Nature* 507 (7492), 346–349.
- Wagner, W., Dorigo, W., de Jeu, R., Fernandez, D., Benveniste, J., Haas, E., Ertl, M., 2012. Fusion of active and passive microwave observations to create an essential climate variable data record on soil moisture. *ISPRS Ann. Photogramm. Remote Sens. Spat. Inf. Sci.* 7, 315–321.
- Walker, J.C.G., Hays, P.B., Kasting, J.F., 1981. A negative feedback mechanism for the long-term stabilization of Earth's surface temperature. *J. Geophys. Res.* 86 (C10), 9776.
- Wang, S., Yeager, K.M., Wan, G., Liu, C.-Q., Liu, F., Lü, Y., 2015. Dynamics of CO<sub>2</sub> in a karst catchment in the southwestern plateau, China. *Environ. Earth Sci.* 73 (5), 2415–2427.
- Yoshimura, K., Nakao, S., Noto, M., Inokura, Y., Urata, K., Chen, M., Lin, P.-W., 2001. Geochemical and stable isotope studies on natural water in the Taroko Gorge karst area, Taiwan—chemical weathering of carbonate rocks by deep source CO<sub>2</sub> and sulfuric acid. *Chem. Geol.* 177 (3), 415–430.
- Yoshimura, K., Liu, Z., Cao, J., Yuan, D., Inokura, Y., Noto, M., 2004. Deep source CO<sub>2</sub> in natural waters and its role in extensive tufa deposition in the Huanglong Ravines, Sichuan, China. *Chem. Geol.* 205 (1), 141–153.
- Zaihua, L., Daoxian, Y., Shiyi, H., 1997. Stable carbon isotope geochemical and hydrochemical features in the system of carbonate–H<sub>2</sub>O–CO<sub>2</sub> and their implications—evidence from several typical karst areas of China. *Acta Geol. Sin. (English Edition)* 71 (4), 446–454.
- Zhao, M., Liu, Z., Li, H.-C., Zeng, C., Yang, R., Chen, B., Yan, H., 2015. Response of dissolved inorganic carbon (DIC) and  $\delta^{13}\text{C}_{\text{DIC}}$  to changes in climate and land cover in SW China karst catchments. *Geochim. Cosmochim. Acta* 165, 123–136.